Eurofleets+

An alliance of European marine research infrastructure to meet the evolving needs of the research and industrial communities

This project has received funding from the European Union's Horizon 2020 research and innovation programme under grant agreement N°. 824077

CRUISE REPORT

Variation in subduction inputs along the Hikurangi subduction margin (VISIT Hikurangi)

RV Tangaroa, Cruise No. TAN2305,

31/03/2023 – 11/04/2023, Wellington (New Zealand) – Wellington (New Zealand)

Sunset over the port side of RV Tangaroa during Cruise TAN2305

Authors:

Crutchley, G., Bell, R., Bassett, D., Berndt, C., Barker, D., Fagereng, Å.

Table of Contents

1 Summary

Cruise TAN2305 was proposed and planned with the aim of collecting 2D seismic reflection data across a broad region of the Hikurangi Plateau (see Section 2 for the objectives). The total time period at sea (approximately ten days) provided us with ~7.5 days of continuous data acquisition that resulted in ~1400 kilometres of seismic profiles (**Fig. 1.1**). There were ~2.5 days of downtime because of adverse weather. Approximately 1000 of the total line kilometres were collected in the planned survey area east of North Island on the Hikurangi Plataeu. Poor weather at the end of the voyage meant that no further data could be collected off the North Island's east coast. To make use of the remaining few days despite the weather, we transited south to collect data in Cook Strait, which was shielded from the worst of the weather (NE winds). The data collected in Cook Strait can support future research planned by the cruise particpants. Overall, the cruise was successful and enabled the collection of sufficient data to tackle each of the research objectives.

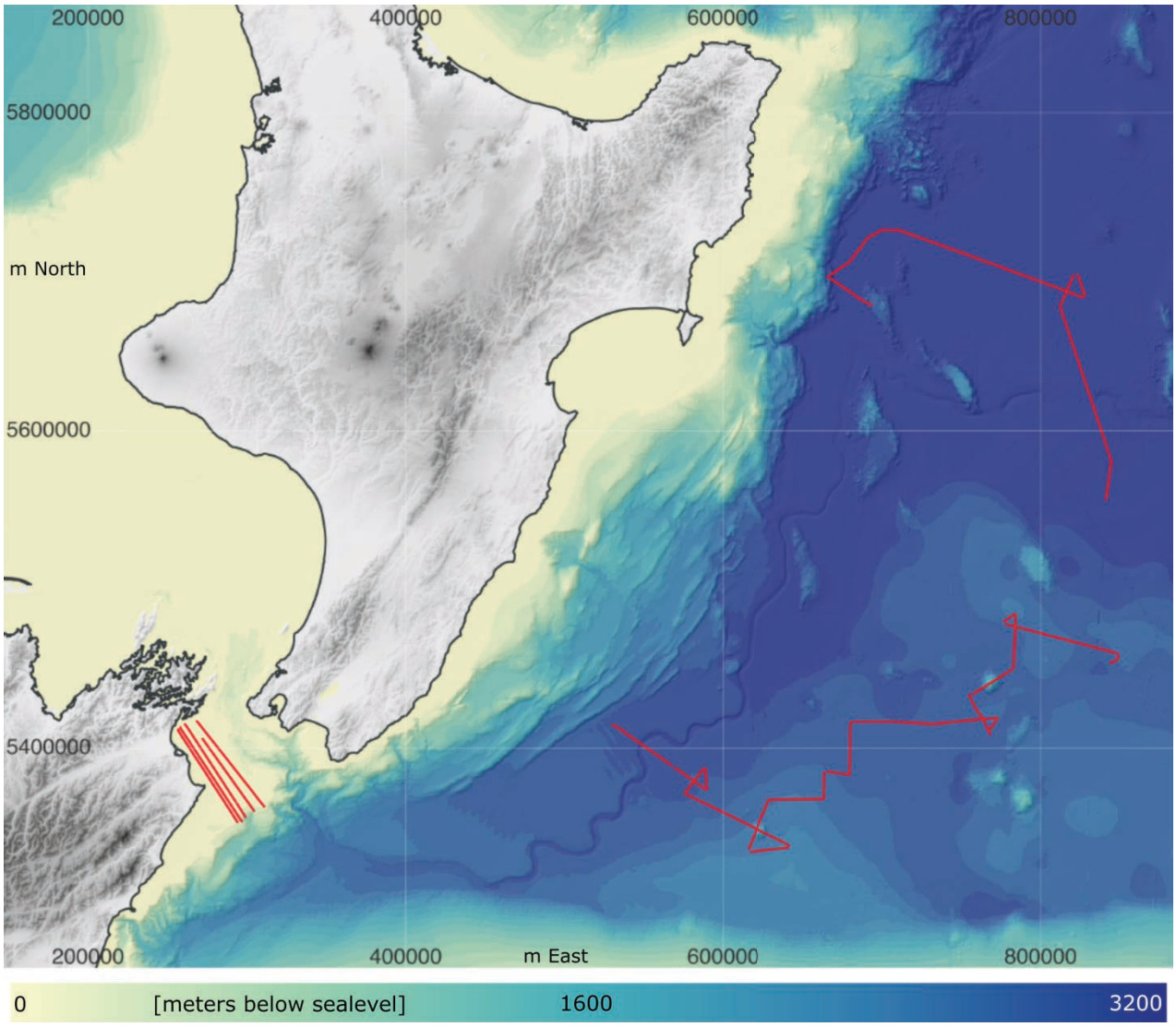

Fig. 1.1 Working area and collected seismic lines (red) of R/V Tangaroa Cruise TAN2305. Bathymetry from New Zealand's National Institute of Water and Atmospheric Research (NIWA). Map coordinates are metres of UTM Zone 60S (WGS84).

2 Research Programme/Objectives

2.1 Background

Subduction plate boundary faults are capable of generating some of the largest earthquakes and tsunami on Earth, such as the magnitude 9.0, 2011 Tōhoku earthquake, Japan. However, in the last two decades a new type of seismic phenomenon has been discovered at subduction zones globally: slow slip events (SSEs). Slow slip events are transient episodes of aseismic slip at a rate intermediate between averaged interplate velocities and the rate required to incite seismic waves (Schwartz and Rokosky, 2007). The physical mechanisms that lead to SSEs remain poorly understood and their potential to trigger highly destructive earthquakes and tsunami on nearby faults is unknown, making slow slip a new and uncharted aspect of earthquake hazard. Resolving what controls whether a plate boundary fault ruptures in large earthquakes or slips slowly is one of the most important challenges in seismology today (Lay, 2009).

The Hikurangi margin, North Island, New Zealand accommodates oblique subduction of the Pacific Plate beneath the Australian Plate at a rate of ~4.5-5.5 cm/yr (**Fig. 2.1**). Despite a lack of major historical or instrumented earthquakes on the subduction plate boundary interface, paleoseismic evidence clearly documents the occurrence of large (>M8) earthquakes on the southern Hikurangi subduction interface in the last 1 kyrs (Clark et al., 2015). Geodetic data reveal that the south Hikurangi plate interface is locked to ~20-30 km depth, with deep SSEs occurring down-dip of this zone between 30 and 45 km depth (Wallace et al., 2012a, **Fig. 2.1**). This deep, strong locking is thought to be a proxy for earthquake potential. The margin exhibits a sharp and profound along-strike transition in interseismic locking at latitude 40°S (**Fig. 2.1**), where in contrast to the south, the north Hikurangi margin is largely unlocked and hosts some of the world's most well characterised shallow SSEs (<2 km below the seabed) (e.g. Wallace and Beavan 2010; Wallace et al., 2016).

The physical properties and processes responsible for controlling the dramatic change in interseismic locking depth and fault slip behaviour at 40°S on the Hikurangi margin are poorly understood. Given similarities in slab age and convergence velocities along the margin, these are unlikely to be the explanation. Other factors that may be responsible include the composition, thickness, and geometry of the subducting sedimentary sequence (Rea and Ruff, 1996; Underwood, 2007), fluid content and permeability of the incoming sediments, oceanic crust, and accretionary prism (Brown et al., 2003; Saffer and Tobin, 2011; Wallace et al., 2012b), incoming plate roughness, including seamounts (Bell et al., 2014; Wang and Bilek, 2014; Ellis et al., 2015), and the architecture of the décollement within sediments on the incoming plate (Chester et al., 2013; Rowe et al., 2013; Barnes et al., 2020).

A considerable amount of seismic reflection data is available along the east coast of North Island, collected primarily to image the shallow parts of the accretionary wedge and decollement. Few profiles cross the deformation front and image substantial parts of the incoming sedimentary section. The existing seismic data reveal that the plate interface in the south, where coupling is high, regionally forms along a high amplitude, continuous reflection which has been named Reflector 7 (R7) (Barnes et al. 2018). This reflector is contained within a thick sedimentary sequence creating a smooth, subducting ocean floor. Based on its seismic facies character and depth, R7 is suspected to be a horizon within pelagic sediments, however, this has not yet been tested with direct sampling by drilling and there are limited seismic data that allow lateral constraints on any variability in the seismic character of R7.

In the north, the structure of the margin is very different. Here the incoming sedimentary section is thinner and heterogeneous with the subduction of rough, seamount studded ocean crust (Barnes et al., 2020). International

Ocean Discovery Program (IODP) Expeditions 372 and 375 in 2017-2018 drilled, logged, and sampled input sediments and a shallow splay fault in north Hikurangi, to specifically target the materials that may host SSEs (Wallace et al., 2019). It revealed that the deeper incoming sedimentary section, where the plate boundary interface forms, is composed of Eocene-Pliocene pelagic sediments (composed of smectite-rich and carbonaceous mudstones) and Cretaceous volcaniclastics (Barnes et al., 2020). In 2017-2018 Bell, Bassett and Fagereng led components of new 3D onshore-offshore (NZ3D) and wide-angle 2D seismic data collection experiments (SHIRE) to produce high-resolution velocity models of the northern slow slip zone and the transition in interseismic coupling.

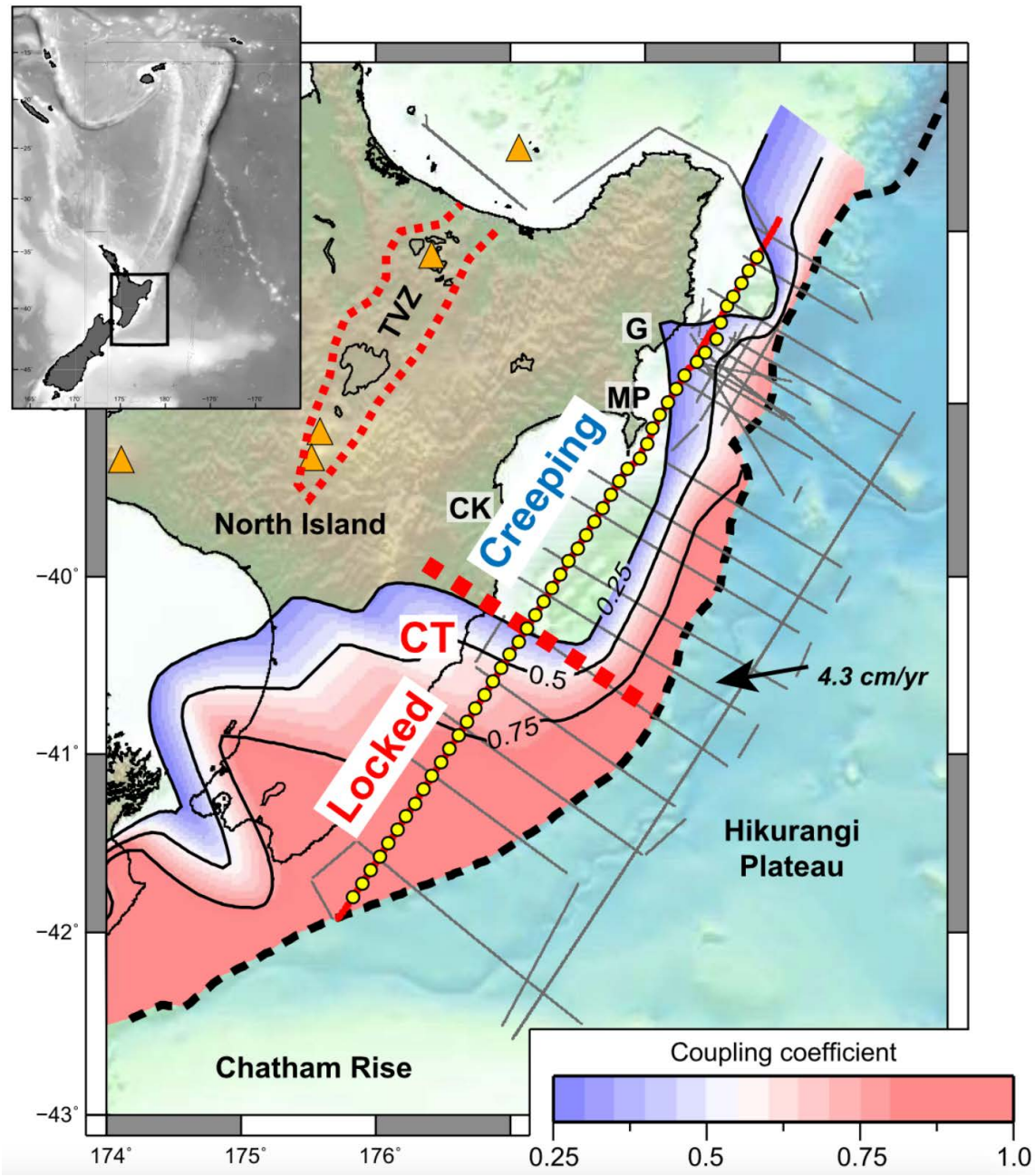

Fig. 2.1 Map of the study area (after Bassett et al. 2022) showing the following: Hikurangi deformation front (heavy broken black line), subduction interface coupling coefficient, existing SHIRE 2D seismic reflection profiles (grey lines), OBS stations on SHIRE strike line (yellow dots), boundary between locked and creeping subduction interface behavior (heavy broken red line). Our seismic surveying targets the Hikurangi Plateau to the east of the deformation front.

2.2 Voyage Aims

Our aim is to test whether along-strike changes in the thickness, composition or physical properties of the Eocene-Pliocene pelagic sediments on the incoming Pacific plate are responsible for the sharp, along-strike differences in interseismic coupling and seismic behaviour observed along the Hikurangi margin, and whether similar changes in sediment properties could be responsible for controlling seismic behaviour at other subduction zones.

In relation to this aim we have the following hypotheses:

Hypothesis 1: The transition from creeping to locked interseismic behaviour is related to physical properties of the incoming sedimentary section.

Hypothesis 2: Variations in fluid pressure control whether a plate interface is interseismically locked or creeping.

In order to fully test these hypotheses VISIT-Hikurangi has the following objectives:

Objective 1: Collect a new seismic reflection dataset involving trench-perpendicular and trench- parallel lines so that the thickness and seismic character of the pelagic sediments and incoming seamounts can be constrained up to 200 km east of the deformation front.

Objective 2: Collect a new trench-parallel seismic reflection profile to correlate R7 to drill site U1520 and analyse changes in R7's seismic reflection character along-strike.

Objective 3: Collect new seismic reflection data that provide appropriate site-survey data for a proposed IODP drilling expedition (proposal 959, Fagereng et al.) to target R7, incoming seamounts, and the pelagic sediments directly.

3 Narrative of the Cruise

31/03/23

- 08:00 Toolbox meeting discussing arrival of science team for VISIT voyage
- 10:00 Safety induction tours for all science party member
- 13:00 Crew Meeting
- 14:00 Departure from Wellington (174°, 47'; -41°, 16')
- 18:00 Ship's clocks changed back one hour

01/04/23

- 01:20 On station ready for deployment of seismic reflection gear
- 02:30 Start of 2D seismic survey
- 12:00 Toolbox meeting. Discussed successful deployment and plans for following days

02/04/23

- 10:30 Meeting for ship's crew
- 11:45 Daily meeting: captain and voyage leader

03/04/23

- 12:00 Toolbox. Continue collecting data as per.
- 16:00 Wind and sea state deteriorating. Deemed OK for collecting data through the night.

04/04/23

- 8:30 Tow cable to the gun broke at the eye. The shackle was continually wearing down the steel cable.
- 8:40 Seismic system recovered due to poor sea state. Forced break in acquisition.

05/04/23

- 4:10 Start of redeployment of seismic system. First the streamer, then the gun, as usual. Deck's crew had placed a thimble in the eye of the steel cable to prevent further wear and potential breakage.
- 5:00 Redeployment completed and data acquisition resumed.
- 5:05 Noticed that the supply cable to the gun was wrapped around the tow cable.
- 5:20 Tow cable and supply cable successfully separated from each other and acquisition resumed. Vessel now approaching start of line.
- 5:30 High streamer leakage. Streamer had to be recovered. The fourth streamer from the end had been stretched and severely damaged. We took it out of the array, which resolved the leakage issue. The system was redeployed with 18 streamers instead of 19.
- 6:45 Collecting data again with the new (shorter) streamer configuration.

06/04/23

- Collecting seismic data uninterrupted.

07/04/23

- 8:30 Seismic system recovered due to worsening sea state.
- 10:00 Decision was made to transit to southern Hikurangi (Cook Strait region), due to the persistence of rough weather in the north. Staying in the north would have had a high risk of no additional data collection, while better weather in the south meant that additional data (beyond the objectives of the VISIT project) could be collected. We decided to use the time in the south to collect data on the western side of Cook Strait, to support future data acquisition planned in this area, also with a seismic hazard focus.

08/04/23

- 16:00 Seismic deployment began.
- 17:00 Deployment complete and data acquisition had begun.

09/04/23

- Seismic acquisition continued all day without interruption.

10/04/23

- 06:00 Variable noise on shot gathers and leakage. System had to be recovered
- 10:30 System re-deployed after removing the fourth streamer section, and then all sections from the fifth section onwards. New acquisition began with just 4 streamer sections (32 channels) and one bird on the stretch.

- 19:00 End of acquisition, recovery of seismic system, packing

11/04/23

- 08:00 Alongside in Wellington harbour
- 08:30 Final toolbox meeting, demobilisation begins
- 14:00 Demobilisation complete (174°, 47’; -41°, 16’)

4 Seismic Acquisition

4.1 Source

We used a GI gun operating in harmonic mode with a 75 cubic-inch generator and 75 cubic-inch injector (**Fig. 4.1**). Pressure supplied to the airgun was nominally set to 150 bar, supplied by NIWA’s Price compressor installed in the centre of the deck and managed by the ship’s crew. The gun was deployed from the fantail of the vessel and secured against the port-stern corner. The distance between the port-stern corner of the vessel and the location of the source in the water was 22 m. There was a further 24.5 m along the length of the ship to the installed GPS position, as well as a 4.7 m offset towards starboard (see **Fig. 4.2**). The gun was towed 2 m beneath the sea surface.

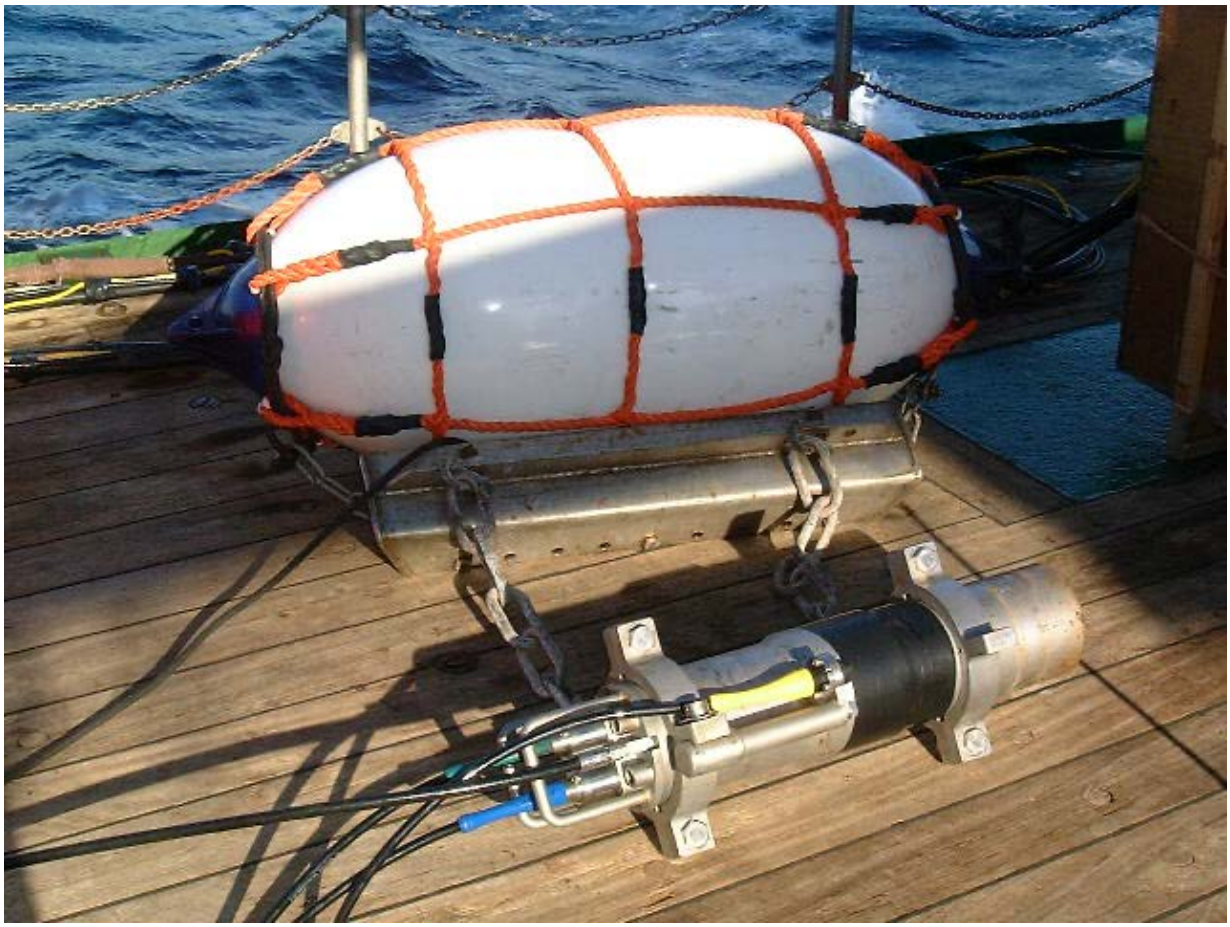

Fig. 4.1 GEOMAR’s GI airgun attached to a deployment frame and a float. Note: photo not from this voyage.

4.2 Receivers

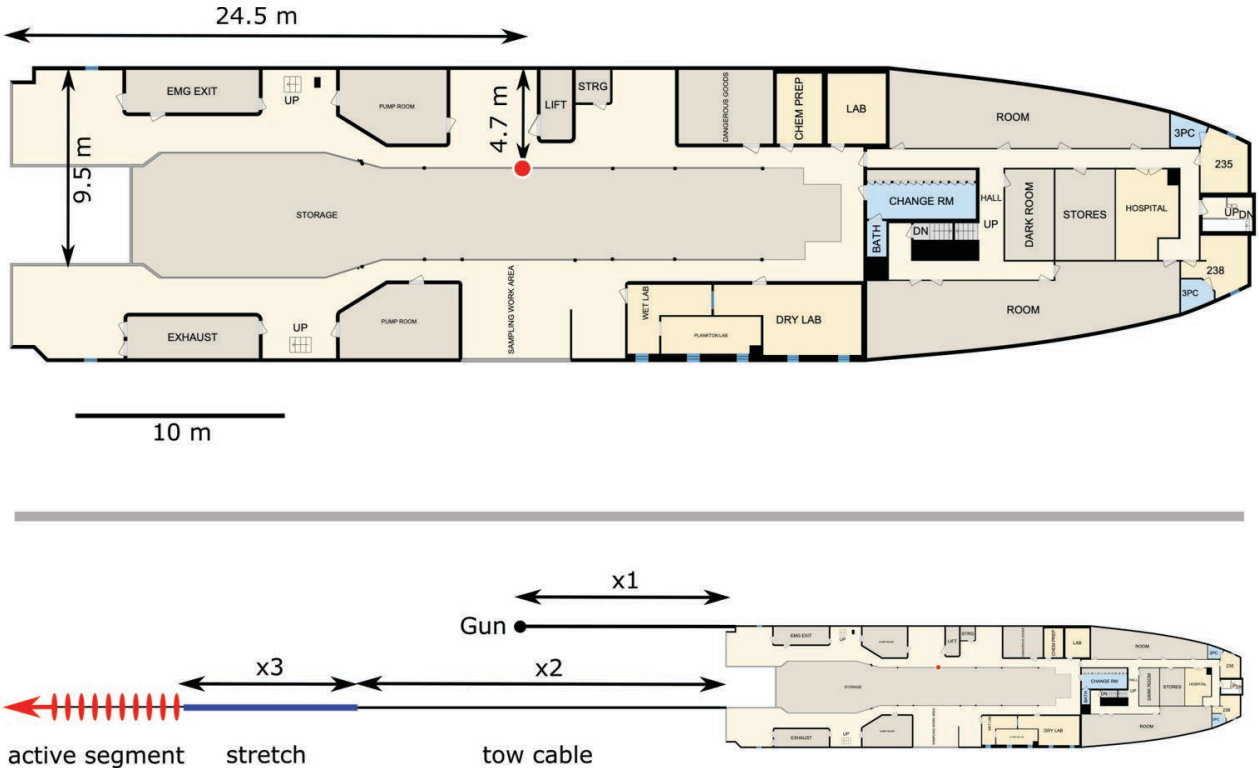

Fig. 4.2 **Top)** Map view of RV Tangaroa's shelter deck. The red dot is the position of our internal GPS receiver, installed 4.7 m inboard of the port side of the vessel, and 24.5 m forward of the vessel's stern. **Bottom)** Distances to the airgun and the start of the active section of the streamer behind the vessel. x1 and x3 were constant for all surveys at 22 m and 20 m, respectively. Distance x2 was 42.5 m for surveys 1010 – 1070 and 54.5 m for surveys 2010 to 6010. Note: There is an additional 0.75 m from the end of the stretch to the first channel. See Table 1 for channel offsets.

The receiver array changed during the voyage due to defective streamer segments that had to be removed. Due to the placement of birds at strategic positions along the streamer, there were locations along the receiver array where the spacing from one channel to the next was 3.125 m (rather than 1.5625 m). The additional 1.5625 m in these locations was taken up by a receiverless segment to which the bird was attached. **Fig. 4.2** depicts the measured offsets from the GPS receiver on the vessel, including the lengths of the tow cable and the stretch segment. We strived for a streamer depth of 2 – 2.5 m beneath the sea surface. During good weather conditions this tow depth was generally well achieved, but periods of increased swell led to more variable streamer depths (e.g. depths reaching 5 m below sea surface). **Table 4.1** shows the soure-receiver offsets (in meters) for all channels in each of the different surveys carried out during the voyage.

Surveys 1010 - 1070																
Chan #	1	2	3	4	5	6	7	8	9	10	11	12	13	14	15	16
Offset	37.50	39.0625	40.6250	42.1875	43.7500	45.3125	46.8750	48.4375	50.0000	51.5625	53.1250	54.6875	56.2500	57.8125	59.3750	60.9375
Chan #	17	18	19	20	21	22	23	24	25	26	27	28	29	30	31	32
Offset	62.5000	64.0625	65.6250	67.1875	68.7500	70.3125	71.8750	73.4375	75.0000	76.5625	78.1250	79.6875	81.2500	82.8125	84.3750	85.9375
Chan #	33	34	35	36	37	38	39	40	41	42	43	44	45	46	47	48
Offset	87.5000	89.0625	90.6250	92.1875	93.7500	95.3125	96.8750	98.4375	100.0000	101.5625	103.1250	104.6875	106.2500	107.8125	109.3750	110.9375
Chan #	49	50	51	52	53	54	55	56	57	58	59	60	61	62	63	64
Offset	112.5000	114.0625	115.6250	117.1875	118.7500	120.3125	121.8750	123.4375	125.0000	126.5625	128.1250	129.6875	131.2500	132.8125	134.3750	135.9375
Chan #	65	66	67	68	69	70	71	72	73	74	75	76	77	78	79	80
Offset	137.5000	139.0625	140.6250	142.1875	143.7500	145.3125	146.8750	148.4375	150.0000	151.5625	153.1250	154.6875	156.2500	157.8125	159.3750	160.9375
Chan #	81	82	83	84	85	86	87	88	89	90	91	92	93	94	95	96
Offset	164.0625	165.6250	167.1875	168.7500	170.3125	171.8750	173.4375	175.0000	176.5625	178.1250	179.6875	181.2500	182.8125	184.3750	185.9375	187.5000
Chan #	97	98	99	100	101	102	103	104	105	106	107	108	109	110	111	112
Offset	189.0625	190.6250	192.1875	193.7500	195.3125	196.8750	198.4375	200.0000	201.5625	203.1250	204.6875	206.2500	207.8125	209.3750	210.9375	212.5000
Chan #	113	114	115	116	117	118	119	120	121	122	123	124	125	126	127	128
Offset	214.0625	215.6250	217.1875	218.7500	220.3125	221.8750	223.4375	225.0000	228.1250	229.6875	231.2500	232.8125	234.3750	235.9375	237.5000	239.0625
Chan #	129	130	131	132	133	134	135	136	137	138	139	140	141	142	143	144
Offset	240.6250	242.1875	243.7500	245.3125	246.8750	248.4375	250.0000	251.5625	253.1250	254.6875	256.2500	257.8125	259.3750	260.9375	262.5000	264.0625
Chan #	145	146	147	148	149	150	151	152								
Offset	265.6250	267.1875	268.7500	270.3125	271.8750	273.4375	275.0000	276.5625								

Surveys 2010 - 2050																
Chan #	1	2	3	4	5	6	7	8	9	10	11	12	13	14	15	16
Offset	47.50	49.0625	50.6250	52.1875	53.7500	55.3125	56.8750	58.4375	60.0000	61.5625	63.1250	64.6875	66.2500	67.8125	69.3750	70.9375
Chan #	17	18	19	20	21	22	23	24	25	26	27	28	29	30	31	32
Offset	72.5000	74.0625	75.6250	77.1875	78.7500	80.3125	81.8750	83.4375	85.0000	86.5625	88.1250	89.6875	91.2500	92.8125	94.3750	95.9375
Chan #	33	34	35	36	37	38	39	40	41	42	43	44	45	46	47	48
Offset	97.5000	99.0625	100.6250	102.1875	103.7500	105.3125	106.8750	108.4375	110.0000	111.5625	113.1250	114.6875	116.2500	117.8125	119.3750	120.9375
Chan #	49	50	51	52	53	54	55	56	57	58	59	60	61	62	63	64
Offset	122.5000	124.0625	125.6250	127.1875	128.7500	130.3125	131.8750	133.4375	135.0000	136.5625	138.1250	139.6875	141.2500	142.8125	144.3750	145.9375
Chan #	65	66	67	68	69	70	71	72	73	74	75	76	77	78	79	80
Offset	147.5000	149.0625	150.6250	152.1875	153.7500	155.3125	156.8750	158.4375	160.0000	161.5625	163.1250	164.6875	166.2500	167.8125	169.3750	170.9375
Chan #	81	82	83	84	85	86	87	88	89	90	91	92	93	94	95	96
Offset	174.0625	175.6250	177.1875	178.7500	180.3125	181.8750	183.4375	185.0000	186.5625	188.1250	189.6875	191.2500	192.8125	194.3750	195.9375	197.5000
Chan #	97	98	99	100	101	102	103	104	105	106	107	108	109	110	111	112
Offset	199.0625	200.6250	202.1875	203.7500	205.3125	206.8750	208.4375	210.0000	211.5625	213.1250	214.6875	216.2500	217.8125	219.3750	220.9375	222.5000
Chan #	113	114	115	116	117	118	119	120	121	122	123	124	125	126	127	128
Offset	224.0625	225.6250	227.1875	228.7500	230.3125	231.8750	233.4375	235.0000	238.1250	239.6875	241.2500	242.8125	244.3750	245.9375	247.5000	249.0625
Chan #	129	130	131	132	133	134	135	136	137	138	139	140	141	142	143	144
Offset	250.6250	252.1875	253.7500	255.3125	256.8750	258.4375	260.0000	261.5625	263.1250	264.6875	266.2500	267.8125	269.3750	270.9375	272.5000	274.0625
Chan #	145	146	147	148	149	150	151	152								
Offset	275.6250	277.1875	278.7500	280.3125	281.8750	283.4375	285.0000	286.5625								

Surveys 4010 - 4040 & 5010																
Chan #	1	2	3	4	5	6	7	8	9	10	11	12	13	14	15	16
Offset	47.50	49.0625	50.6250	52.1875	53.7500	55.3125	56.8750	58.4375	60.0000	61.5625	63.1250	64.6875	66.2500	67.8125	69.3750	70.9375
Chan #	17	18	19	20	21	22	23	24	25	26	27	28	29	30	31	32
Offset	72.5000	74.0625	75.6250	77.1875	78.7500	80.3125	81.8750	83.4375	85.0000	86.5625	88.1250	89.6875	91.2500	92.8125	94.3750	95.9375
Chan #	33	34	35	36	37	38	39	40	41	42	43	44	45	46	47	48
Offset	97.5000	99.0625	100.6250	102.1875	103.7500	105.3125	106.8750	108.4375	110.0000	111.5625	113.1250	114.6875	116.2500	117.8125	119.3750	120.9375
Chan #	49	50	51	52	53	54	55	56	57	58	59	60	61	62	63	64
Offset	122.5000	124.0625	125.6250	127.1875	128.7500	130.3125	131.8750	133.4375	135.0000	136.5625	138.1250	139.6875	141.2500	142.8125	144.3750	145.9375
Chan #	65	66	67	68	69	70	71	72	73	74	75	76	77	78	79	80
Offset	147.5000	149.0625	150.6250	152.1875	153.7500	155.3125	156.8750	158.4375	160.0000	161.5625	163.1250	164.6875	166.2500	167.8125	169.3750	170.9375
Chan #	81	82	83	84	85	86	87	88	89	90	91	92	93	94	95	96
Offset	174.0625	175.6250	177.1875	178.7500	180.3125	181.8750	183.4375	185.0000	186.5625	188.1250	189.6875	191.2500	192.8125	194.3750	195.9375	197.5000
Chan #	97	98	99	100	101	102	103	104	105	106	107	108	109	110	111	112
Offset	199.0625	200.6250	202.1875	203.7500	205.3125	206.8750	208.4375	210.0000	211.5625	213.1250	214.6875	216.2500	217.8125	219.3750	220.9375	222.5000
Chan #	113	114	115	116	117	118	119	120	121	122	123	124	125	126	127	128
Offset	224.0625	225.6250	227.1875	228.7500	230.3125	231.8750	233.4375	235.0000	238.1250	239.6875	241.2500	242.8125	244.3750	245.9375	247.5000	249.0625
Chan #	129	130	131	132	133	134	135	136	137	138	139	140	141	142	143	144
Offset	250.6250	252.1875	253.7500	255.3125	256.8750	258.4375	260.0000	261.5625	263.1250	264.6875	266.2500	267.8125	269.3750	270.9375	272.5000	274.0625

Survey 6010																
Chan #	1	2	3	4	5	6	7	8	9	10	11	12	13	14	15	16
Offset	47.50	49.0625	50.6250	52.1875	53.7500	55.3125	56.8750	58.4375	60.0000	61.5625	63.1250	64.6875	66.2500	67.8125	69.3750	70.9375
Chan #	17	18	19	20	21	22	23	24	25	26	27	28	29	30	31	32
Offset	72.5000	74.0625	75.6250	77.1875	78.7500	80.3125	81.8750	83.4375	85.0000	86.5625	88.1250	89.6875	91.2500	92.8125	94.3750	95.9375

Table. 4.1 Receiver offset tables for different surveys. Vertical red lines represent the positions of the birds in the spread. Note that the birds take up 1.5625 m of space, which is why the spacing from a receiver before a bird to a receiver after a bird is 3.125 m, rather than the standard 1.5625 m spacing.

4.3 Seismic recording parameters

Seismic data were recorded in SEG-D format, with a separate file for every shot. For the bulk of the surveying, the air-gun was triggered every 9 seconds and data were recorded to a trace length of 8 seconds with the Geometrics recording system. For the last two days of surveying (in Cook Strait) the shot spacing was set to 5 seconds and the

trace length to 4 seconds, due to the shallow water depths. The sampling rate for all surveying was set to 1 ms (1000 Hz). Shot files were written directly to the hard-drive of the acquisition computer and synchronized (on the fly) to a seismic processing computer that was networked with the acquisition computer. The acquisition computer also wrote out a text file with the GPS time for each shot. Position data were recorded at the GPS site installed on the vessel (see **Fig. 4.2**) and were written to text files every second. In addition to this text file, another file was written with the GPS position at the time of triggering the airgun. The precise timing of airgun triggering was controlled by a Longshot gun controller, which was set to have an "aiming point" of 50 ms, which means the peak energy recorded at the gun's hydrophone should be 50 ms after the trigger time. By observing the auxiliary traces in Geometrics we noted that there was an additional 100 ms delay introduced by Geometrics, resulting in a total recording delay of 150 ms. It was unclear to us why there was an additional 100 ms delay introduced by the Geometrics software. Geometrics recorded four additional auxiliary channels per shot, which are written into the segd files. One of these auxiliary channels shows the nearfield waveform from the airgun's hydrophone. Inspection of this waveform showed the peak of the signal to be aligned at 150 ms, which corresponds to the recording delay that needs to be corrected for during processing.

5 Seismic processing

5.1 GEOMAR computer

Our processing sequence comprised the following main steps:

1. Convert SEG-D to Seismic Unix format (*.su)
2. Add dummy traces between channels 80 and 81 and 120 and 121 (to account for gaps at the birds) (as required, depending on length of receiver array – see Table 1)
3. Define shot and receiver geometry in UTM60S coordinate system
4. Crooked line CMP binning
5. Source, receiver and CMP coordinates written to headers of seismic unix shot files
6. Shots filtered with a zero-phase sine-squared filter: Bandpass: 24,48,650,850 Hz
7. Gain recovery: Trace amplitudes multiplied by t^1
8. Amplitude normalization
9. Static shift: Traces moved up by 150 ms
10. Sort to CMP, normal moveout correction (1500 m/s constant velocity)
11. Stack
12. Spherical divergence (1500 m/s, Vpower = 2.0, Tpower = 1.0)
13. Balance amplitudes (entire trace, amplitude)
14. Stolt migration (1500 m/s constant velocity)
15. UTM60S (WGS84) CMP coordinates written to header words 181 (X) and 185 (Y), in centimetres.
16. NZTM CMP coordinates written to header words 73 (X) and 77 (Y), in metres.
17. Write to segy

5.2 GNS computer

In addition to this sequence, we used the GNS Science processing workstation to carry out additional processing with the Globe Claritas processing software. The additional processing steps applied were as follows:

- FK filtering of shot gathers (between Steps 9 and 10)
- Semblance smoothing coherency filter (after FK filtering)
- Horizontal automatic despiking on channel gathers (only on lines 1060, 1070 and 2010, as required)

- Horizontal automatic despiking on NMO-corrected CMP gathers (after Step 10)
- Debias (before stacking)
- Finite difference migration (1500 m/s constant velocity) (instead of Step 14)

5.3 Acquisition and Processing parameters

Table 5.1 displays the key acquisition and processing parameters applied for the 29 seismic lines collected during the cruise.

Proc ID	Line ID	CDPi	CDPn	Bin	Shoti	Shotn	Chan	S	L	Sz	Rz	1st CDPX	1st CDPY	last CDPX	last CDPY	Near	Far	Sx
P1010_340_2550	TAN2305-01	4	7197	6.25	340	2550	152	1	8	2	2.5	530323.2	5414417.9	567089	5389346.6	37.5	276.5	9
P1010_2560_3695	TAN2305-02	5	3788	6.25	2560	3695	152	1	8	2	2.5	569636.8	5387576.3	588825.6	5373930.9	37.5	276.5	9
T01_3784_4484	TAN2305-03	5	2103	6.25	3784	4484	152	1	8	2	2.5	589734.4	5374702.7	587796.8	5387039.4	37.5	276.5	9
P1020_4500_5480	TAN2305-04	5	3073	6.25	4500	5480	152	1	8	2	2.5	587554.7	5386915.8	576035.6	5371759.4	37.5	276.5	9
P1030_5500_9080	TAN2305-05	5	11841	6.25	5500	9080	152	1	8	2	2.5	576073.6	5371471.4	642018	5338591.7	37.5	276.5	9
T02_9215_10857	TAN2305-06	4	3834	6.25	9215	10857	152	1	8	2	2.5	641170.6	5337085.8	617503.6	5334548.2	37.5	276.5	9
P1040_11050_12540	TAN2305-07	5	5284	6.25	11050	12540	152	1	8	2	2.5	616243.8	5336825.9	629045.4	5367124.8	37.5	276.5	9
P1050_12590_14180	TAN2305-08	5	5366	6.25	12590	14180	152	1	8	2	2.5	629938.4	5367401	663327.3	5367859.2	37.5	276.5	9
P1060_14220_14985	TAN2305-09	5	2612	6.25	14220	14985	152	1	8	2	2.5	663831.7	5368279.4	664185.3	5384466.6	37.5	276.5	9
P1070_15115_15711	TAN2305-10	5	2175	6.25	15115	15711	152	1	8	2	2.5	666517.3	5385072.6	679873.3	5383249.9	37.5	276.5	9
P2010_16239_17794	TAN2305-11	5	5167	6.25	16239	17794	152	1	8	2	2.5	679961.4	5383745.3	680579.5	5415896.3	49.5	288.5	9
P2020_17890_21837	TAN2305-12	5	14638	6.25	17890	21837	152	1	8	2	2.5	681953.9	5416540.8	772902.6	5418685.4	49.5	288.5	9
T03_21864_22264	TAN2305-13	4	1296	6.25	21864	22264	152	1	8	2	2.5	772849.9	5418383.4	768202	5411897.6	49.5	288.5	9
P2030_22533_23910	TAN2305-14	5	4502	6.25	22533	23910	152	1	8	2	2.5	768297.4	5408702.1	755316.3	5433348.5	49.5	288.5	9
P2040_24038_27010	TAN2305-15	5	10212	6.25	24038	27010	152	1	8	2	2.5	757638.7	5434190.1	784418.4	5483832.3	49.5	288.5	9
T04_27096_27472	TAN2305-16	5	1293	6.25	27096	27472	152	1	8	2	2.5	783501.9	5484345.6	777112.4	5479719	49.5	288.5	9
P2050_27596_30963	TAN2305-17	5	11560	6.25	27596	30963	152	1	8	2	2.5	778556.2	5477973.1	848210.9	5459642.9	49.5	288.5	9
T05_31085_31495	TAN2305-18	4	1230	6.25	31085	31495	152	1	8	2	2.5	848837.2	5458079.4	843907.9	5453612.8	49.5	288.5	9
P4010_34400_35900	TAN2305-19	5	5226	6.25	34400	35900	144	1	8	2	2.5	693530.7	5679103.4	666397.2	5696970.2	49.5	276	9
P4020_36080_39113	TAN2305-20	5	8876	6.25	36080	39113	144	1	8	2	2.5	668262.4	5698130.6	710951.6	5726222.1	49.5	276	9
P4030_39114_44870	TAN2305-21	5	19699	6.25	39114	44870	144	1	8	2	2.5	710859.8	5726223.4	826291.8	5684077.4	49.5	276	9
T06_44970_45650	TAN2305-22	5	2269	6.25	44970	45650	144	1	8	2	2.5	827757.4	5684902.4	823261.1	5698171.5	49.5	276	9
P4040_45800_53858	TAN2305-23	5	23690	6.25	45800	53858	144	1	8	2	2.5	820470	5697475.8	841178.4	5556788.5	49.5	276	9
P5010_54590_60140	TAN2305-24	1	44487	1.5625	54590	60140	144	1	4	2	2	293916.3	5353489.3	256746.4	5411763.2	49.5	276	5
P5020_60630_66087	TAN2305-25	1	37364	1.5625	60630	66087	144	1	4	2	2	261009.8	5414970.2	292892.6	5366299.8	49.5	276	5
P5020b_67000_67840	TAN2305-26	1	6285	1.5625	67000	67840	144	1	4	2	2	293769	5364953.9	299031.8	5356762.6	49.5	276	5
P5030_68200_74820	TAN2305-27	1	45454	1.5625	68200	74820	144	1	4	2	2	296893.3	5353968.3	258100.2	5413038.7	49.5	276	5
P5040_75831_81135	TAN2305-28	1	43734	1.5625	75831	81135	144	1	4	2	2	268613.2	5416887	310763.2	5363288	49.5	276	5
P6010_83280_89968	TAN2305-29	1	35668	1.5625	83280	89968	32	1	4	2	2	304411	5360693.8	272104.7	5405813.1	49.5	99.5	5

Table. 5.1 Acquisition and processing paarmeters for all lines. ProcID = ID assigned for processing; Line ID = final line ID; CDPi = first CDP number; CDPn = last CDP number; Bin = CDP bin size (m); Shoti = first shot number; Shotn = last shot number; Chan = number of channels; S = sample rate (ms); L = trace length (seconds); Sz = nominal source depth (m); Rz = noiminal receiver depth (m); 1st CDPX (X coordinate for 1st CDP; 1st CDPY (Y coordinate for 1st CDP; last CDPX (X coordinate for last CDP; last CDPY (X coordinate for last CDP; Near = near offset (m); Far = far offset (m); Sx = shot rate (s). Note: ccordinates are UTM60S (WGS84 datum) (EPSG: 32760).

5.4 Acquisition and Processing parameters

The following important header words are stored in all stacked seismic sections, including the final migrated sections (Table 5.2).

Header Name	Bytes	Description
CDP	21-24	CDP number
SOURCE_X	73-76	X coordinate of CDP in NZTM coordinates (EPSG: 2193), in **metres**
SOURCE_Y	77-80	Y coordinate of CDP in NZTM coordinates (EPSG: 2193), in **metres**
SAMP_RATE	117-118	Sample rate (1000 microseconds)
YEAR	157-158	Year
DAY	159-160	Day
HOUR	161-162	Hour
MINUTE	163-164	Minute
SECOND	165-166	Second
CDP_X	181-184	X coordinate of CDP in UTM60S (WGS84) (EPSG: 32760), in **centimeters**
CDP_Y	185-188	Y coordinate of CDP in UTM60S (WGS84) (EPSG: 32760), in **centimeters**

Table. 5.2 Important header words for processed segy files.

6 Preliminary Results

Onboard processing progressed through to migrated seismic sections for all data that we collected. **Fig. 6.1** shows the distribution of seismic reflection lines acquired during this cruise, together with existing 2D seismic data in the region. Of particular interest is the spatial distribution of the TAN2305 lines with respect to seismic lines collected during Cruise TAN2104 (Bassett et al. 2021). Our TAN2305 dataset was collected to be complementary to the TAN2104 data, including strategic crossing lines and a design that ensured good regional coverage from north to south in the study area. **Fig. 6.2** displays a comparison of our TAN2305 data with the TAN2104 data, in a location where the two datasets cross each other at ~90 degrees (see **Fig. 6.1** for location). **Figures 6.3 – 6.6** provide additional examples of the TAN2305 data, at selected locations (see **Fig. 6.1**).

These examples below provide illustrations for how the project aims are being met through the acquisition and planned analysis. We imaged Sequence-Y broadly in the dataset (e.g. Figs 6.3 and 6.4), including at depths shallower than the proposed drill sites in IODP proposal 959-pre (< 1 s two-way time beneath the seafloor), making drilling more feasible. These data will also be used in further work to map and characterise Sequence-Y regionally. Collectively, the TAN2104 and TAN2305 lines allow the character of Sequence-Y, and the rest of the pelagic input sequence, to be traced along-strike for the full length of the deformation front. Other lines show examples of seamounts, including crossing-lines to better understand their geometry and improve potential scientific drilling targets (e.g. Fig. 6.6).

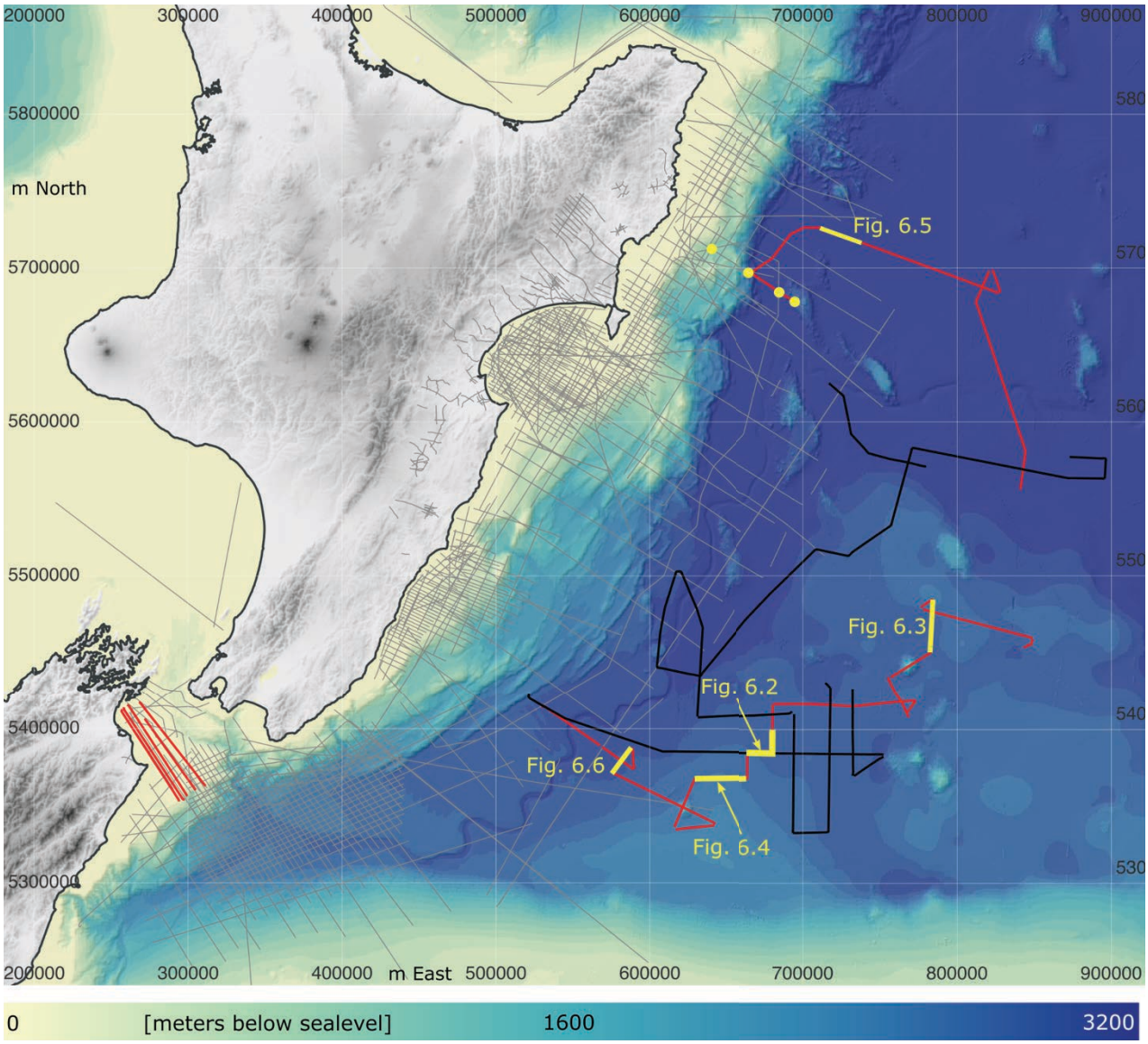

Fig. 6.1 Map of collected seismic lines (red lines). Black lines are seismic profiles from Voyage TAN2104 (Bassett et al. 2021). Faint grey lines are other regional 2D seismic lines. Yellow dots are IODP Expedition 375 drill sites. Coordinates are UTM Zone 60S (metres; WGS84 datum). Locations of selected parts of seismic lines shown in subsequent figures are shown by thick yellow lines.

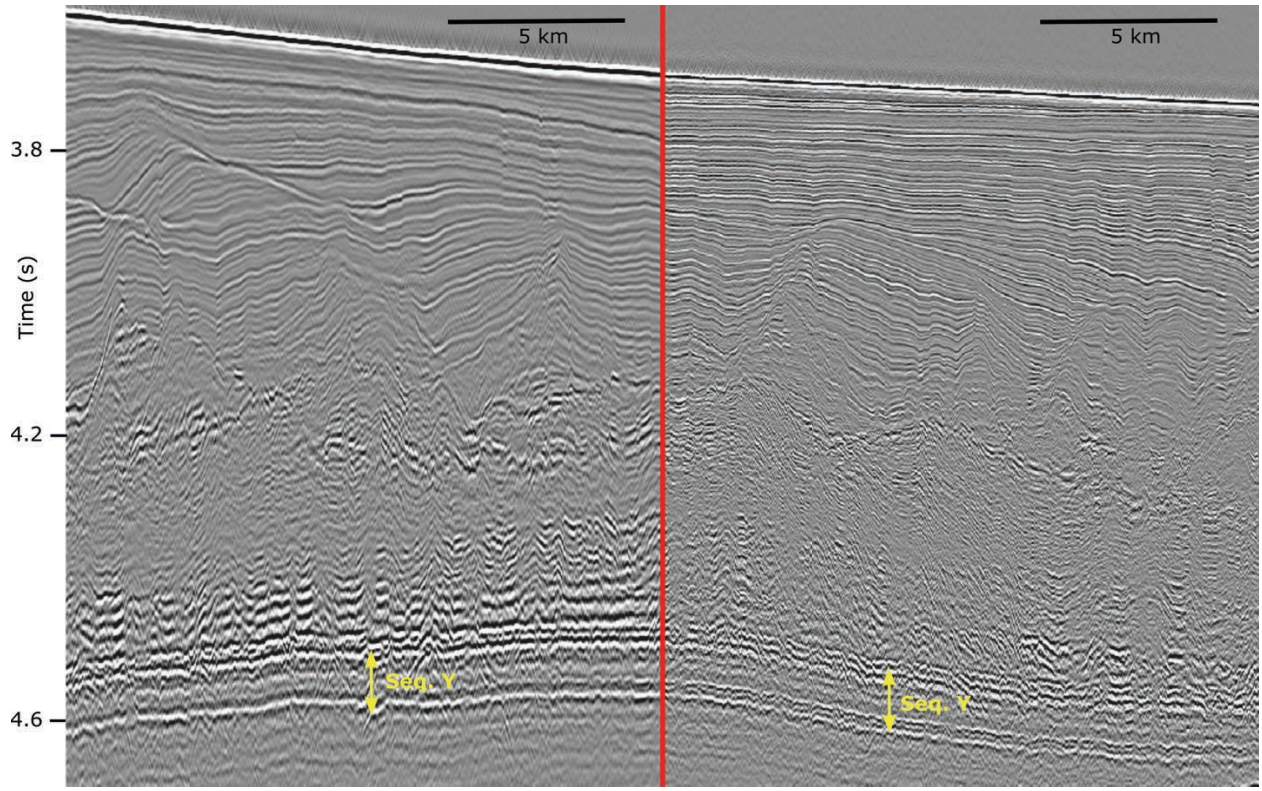

Fig. 6.2 Comparison between data from TAN2104 (left of red line; Line TAN2104-101) and data from this cruise (right of red line; TAN2305-11), at a location where the lines cross each other (see Fig. 6.1 for location). TAN2104 data have better depth penetration, while TAN2305 data have broader frequency content. Black bars show horizontal scales. Approximate extent of Sequence-Y annotated.

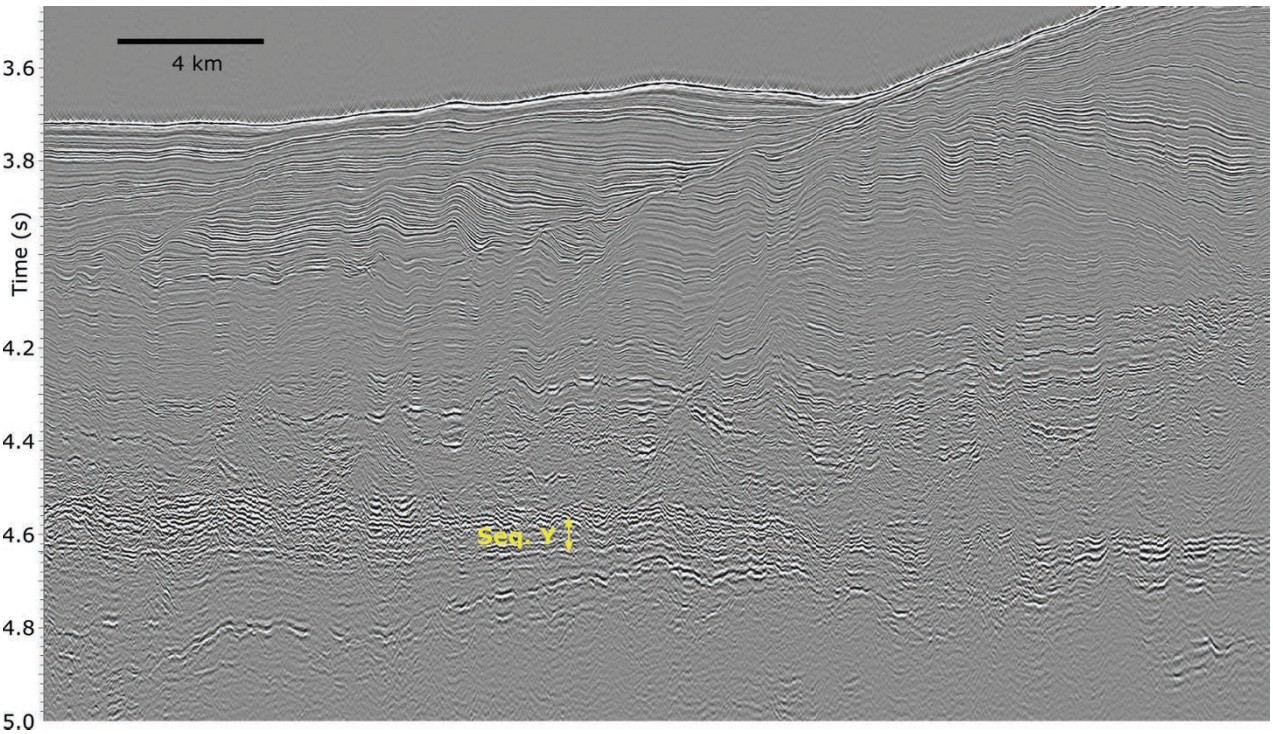

Fig. 6.3 Example part of Seismic Line TAN2305-15 (see Fig. 6.1 for location). Approximate extent of Sequence-Y annotated.

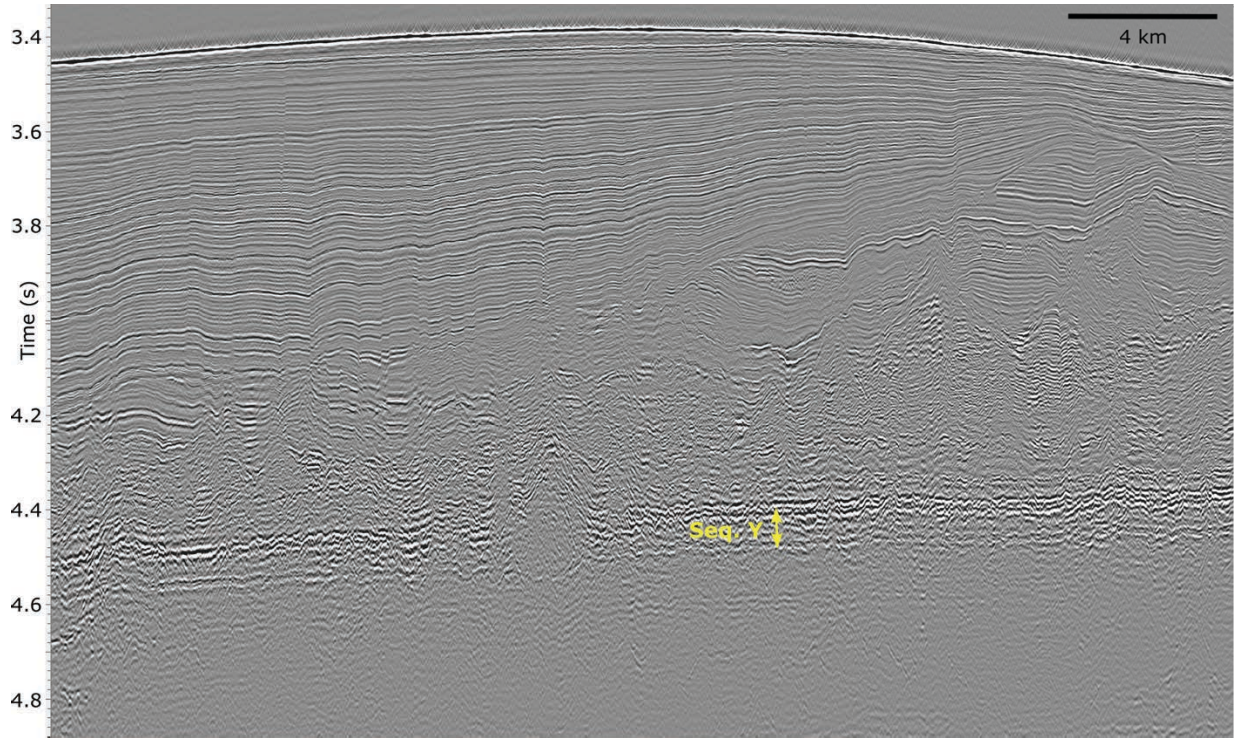

Fig. 6.4 Example part of Seismic Line TAN2305-08 (see Fig. 6.1 for location). Approximate extent of Sequence-Y annotated.

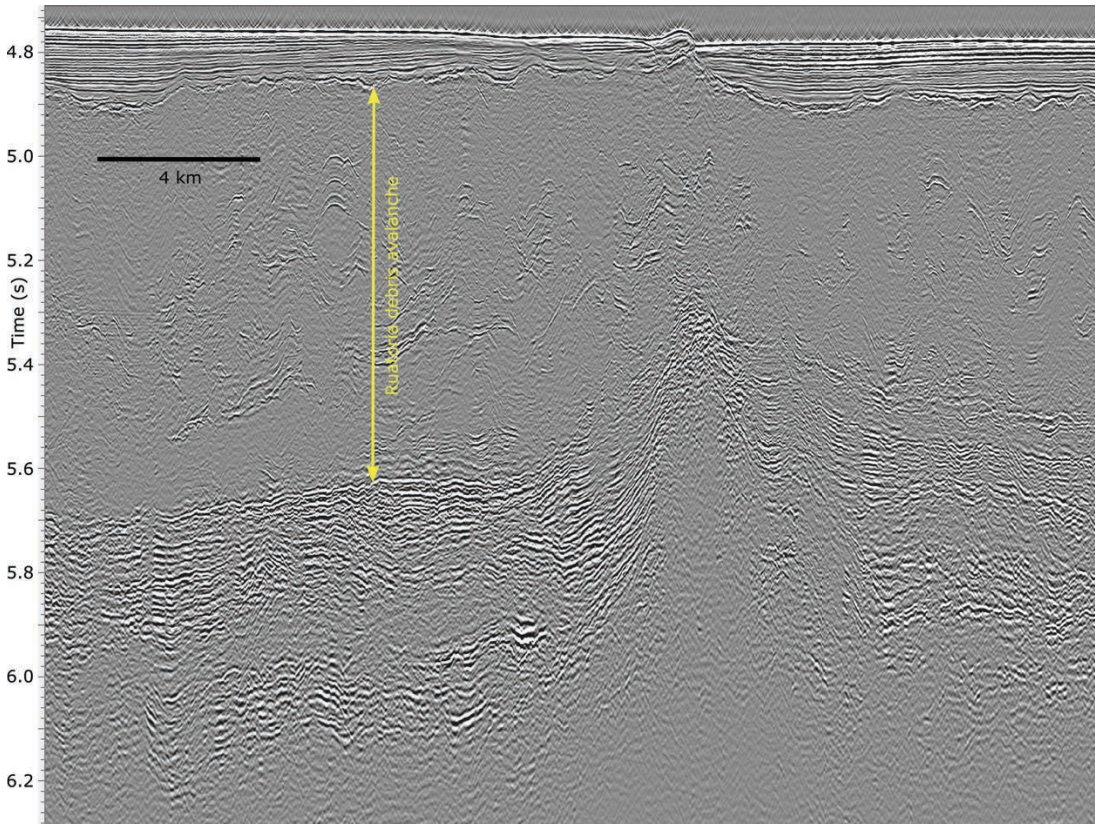

Fig. 6.5 Example part of Seismic Line TAN2305-21 (see Fig. 6.1 for location) imaging disturbed sediments of the Ruatoria Debris Avalanche.

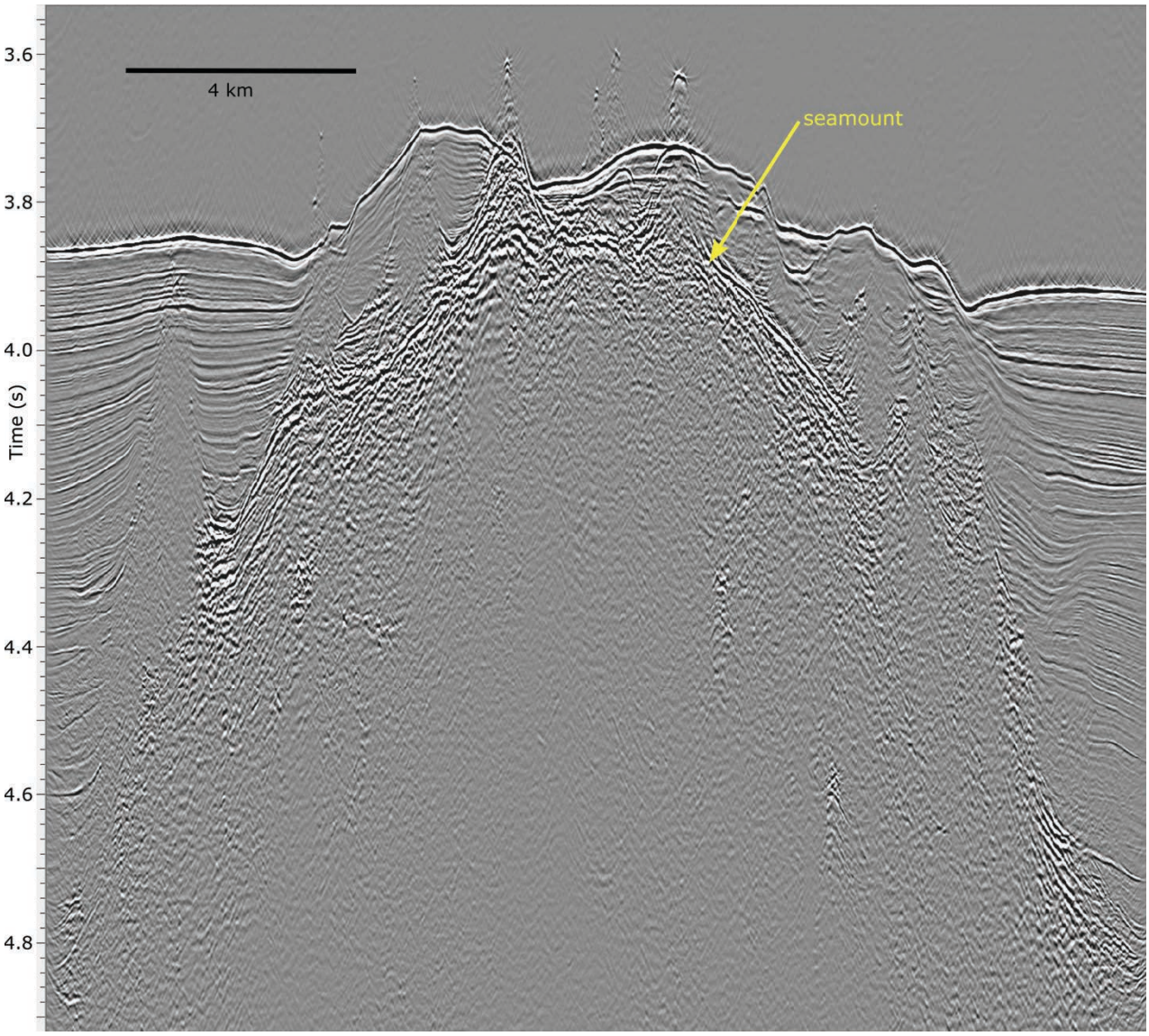

Fig. 6.6 Example part of Seismic Line TAN2305-21 (see Fig. 6.1 for location) with seamount extending through sediment cover to the seafloor.

7 Data and Sample Storage / Availability

Full copies of all data collected during the cruise were made and distributed among all project partners. The data have now been archived at the particpating institutions. We are working on standard metadata for all seismic data that will be uploaded to an online repository, together with the raw and processed data.

8 Science Team

No.	Name	Early career (Y/N)	Gender	Affiliation	Tasks
1	Rebecca Bell	N	F	IC	Project Lead (onshore)*
2	Gareth Crutchley	N	M	GEOMAR	Cruise Lead
3	Dan Bassett	N	M	GNS	Cruise Co-lead
4	Christian Berndt	N	M	GEOMAR	Seismics
5	Åke Fagereng	N	M	CARDIFF	Seismics
6	Bruna Pandolpho	Y	F	GEOMAR	Seismics
7	Laura Frahm	Y	F	IC	Seismics
8	Amy Woodward	Y	F	IC	Seismics
9	Henrike Timm	Y	F	GEOMAR	Seismics
10	Dan Barker	N	M	GNS	Seismics
11	Gero Wetzel	N	M	GEOMAR	Seismics (technician)

*Could not join the cruise due to childcare responsibilities

Affiliations in full:

IC -> Imperial College, London, UK

GEOMAR -> GEOMAR Helmholtz Centre for Ocean Research Kiel, Germany

GNS -> GNS Science, Lower Hutt, New Zealand

CARDIFF -> Cardiff University, Cardiff, UK

9 Acknowledgements

We thank the master of RV Tangaroa (Mark Hansen) and the entire crew for their excellent support during the cruise. We are grateful to Karen Keddy, Ross Mitchell, Rob Christie and Will Quinn for their shore-based support in Wellington. In addition to funding provided by Eurofleets, this cruise was supported financially by each of the participating project partners, as well as the UK National Environment Research Council. This additional funding made the cruise possible in the face of major (unforeseen) increases in logistical costs. We thank all funding agencies and institutes for their contributions. In particular, our thanks go to Bernadette Ni Chonghaile and Niamh Flavin from Eurofleets for their flexibility and support with planning this cruise. We also thank Hui Jia (Imperial College), Mahesh Pillai (Imperial College), Kirsten Hoppe (GEOMAR), Anna Jellie (GNS Science), Yasmin Gregory (Cardiff) and Rob Christie (NIWA) for their hard work in establishing and finalising the various contracts required for this multi-national project.

10 References

Barnes, P.M., Ghisetti, F.C., Ellis, S. and Morgan, J.K., 2018. The role of protothrusts in frontal accretion and accommodation of plate convergence, Hikurangi subduction margin, New Zealand. *Geosphere*, *14*(2), pp.440-468.

Barnes, P.M., Wallace, L.M., Saffer, D.M., and IODP Expedition 372 and 375 Scientists, 2020. Slow slip source characterized by lithological and geometric heterogeneity. *Science Advances, 6*(13), p.eaay3314.

Bell, R., Holden, C., Power, W., Wang, X. and Downes, G., 2014. Hikurangi margin tsunami earthquake generated by slow seismic rupture over a subducted seamount. *Earth and Planetary Science Letters*, *397*, pp.1-9.

Brown, K.M., Kopf, A., Underwood, M.B. and Weinberger, J.L., 2003. Compositional and fluid pressure controls on the state of stress on the Nankai subduction thrust: A weak plate boundary. *Earth and Planetary Science Letters*, *214*(3-4), pp.589-603.

Chester, F.M., Rowe, C., Ujiie, K., Kirkpatrick, J., Regalla, C., Remitti, F., Moore, J.C., Toy, V., Wolfson-Schwehr, M., Bose, S. and Kameda, J., 2013. Structure and composition of the plate-boundary slip zone for the 2011 Tohoku-Oki earthquake. *Science*, *342*(6163), pp.1208-1211.

Clark, K.J., Hayward, B.W., Cochran, U.A., Wallace, L.M., Power, W.L. and Sabaa, A.T., 2015. Evidence for past subduction earthquakes at a plate boundary with widespread upper plate faulting: Southern Hikurangi margin, New Zealand. *Bulletin of the Seismological Society of America*, *105*(3), pp.1661-1690.

Ellis, S., Fagereng, Å., Barker, D., Henrys, S., Saffer, D., Wallace, L., Williams, C. and Harris, R., 2015. Fluid budgets along the northern Hikurangi subduction margin, New Zealand: The effect of a subducting seamount on fluid pressure. *Geophysical Journal International*, *202*(1), pp.277-297.

Ake Fagereng, Dan Bassett, Rebecca Bell, Heather Savage, Laura Wallace, Ryuta Arai, Nathan Bangs, Daniel Barker, Philip Barnes, Gareth Crutchley, Robert Harris, Stuart Henrys, Matt Ikari, Hiroko Kitajima, Shuichi Kodaira, Greg Moore, Demian Saffer, Evan Solomon, Kohtaro Ujiie, Michael Underwood. 2019. Probing the physical controls on a locked vs. creeping megathrust with ocean drilling, Hikurangi Subduction Margin, NZ. IODP pre-proposal 959-Pre.

Lay, T., ed. 2009. *Seismological Grand Challenges in Understanding Earth's Dynamic Systems*. Report to the National Science Foundation, iriS consortium, 76 pp.

Rea, D.K. and Ruff, L.J., 1996. Composition and mass flux of sediment entering the world's subduction zones: Implications for global sediment budgets, great earthquakes, and volcanism. *Earth and Planetary Science Letters*, *140*(1-4), pp.1-12.

Rowe, C.D., Moore, J.C., Remitti, F. and IODP Expedition 343/343T Scientists, 2013. The thickness of subduction plate boundary faults from the seafloor into the seismogenic zone. *Geology*, *41*(9), pp.991-994.

Saffer, D.M. and Tobin, H.J., 2011. Hydrogeology and mechanics of subduction zone forearcs: Fluid flow and pore pressure. *Annual Review of Earth and Planetary Sciences*, *39*, pp.157-186.

Schwartz, S.Y. and Rokosky, J.M., 2007. Slow slip events and seismic tremor at circum-Pacific subduction zones. *Reviews of Geophysics*, *45*(3).

Underwood, M.B., 2007. 3. Sediment inputs to subduction zones. In *The seismogenic zone of subduction thrust faults*(pp. 42-85). Columbia University Press.

Wallace, L.M. and Beavan, J., 2010. Diverse slow slip behavior at the Hikurangi subduction margin, New Zealand. *Journal of Geophysical Research: Solid Earth*, *115*(B12).

Wallace, L.M., Beavan, J., Bannister, S. and Williams, C., 2012a. Simultaneous long-term and short-term slow slip events at the Hikurangi subduction margin, New Zealand: Implications for processes that control slow slip event occurrence, duration, and migration. *Journal of Geophysical Research: Solid Earth*, *117*(B11).

Wallace, L.M., Fagereng, Å. and Ellis, S., 2012b. Upper plate tectonic stress state may influence interseismic coupling on subduction megathrusts. *Geology, 40*(10), pp.895-898.

Wallace, L.M., Webb, S.C., Ito, Y., Mochizuki, K., Hino, R., Henrys, S., Schwartz, S.Y. and Sheehan, A.F., 2016. Slow slip near the trench at the Hikurangi subduction zone, New Zealand. *Science*, *352*(6286), pp.701-704.

Wallace, L., Saffer, D.M., Pecher, I., Petronotis, K., LeVay, L.J. and Expeditions, I.O.D.P., 2019. Hikurangi subduction margin coring, logging, and observatories. *Proceedings of the international ocean discovery program*, *372*.

Wang, K. and Bilek, S.L., 2014. Invited review paper: Fault creep caused by subduction of rough seafloor relief. *Tectonophysics*, *610*, pp.1-24.